



Enhanced Chemotherapeutic Toxicity of Cyclodextrin Templated Size-Tunable Rhodamine 6G nanoGUMBOS

Journal:	<i>Journal of Materials Chemistry B</i>
Manuscript ID	TB-ART-04-2018-001115.R1
Article Type:	Paper
Date Submitted by the Author:	19-Jul-2018
Complete List of Authors:	<p>Bhattacharai, Nimisha; Louisiana State University Department of Chemistry Chen, Mi; Louisiana State University Department of Chemistry Perez, Rocio; Louisiana State University Department of Chemistry Ravula, Sudhir; Louisiana State University Baton Rouge, Department of Chemistry Chhotaray, Pratap; Indian Institute of Technology Delhi; Louisiana State University Baton Rouge, Department of Chemistry Hamdan, Suzana; University of Miami School of Medicine, Biochemistry and Molecular Biology; Louisiana State University Department of Chemistry McDonough, Karen; Louisiana State University, AgCenter Biotechnology Labs Tiwari, Suman ; University of Louisiana at Monroe, Biology Warner, Isiah; Louisiana State University, Department of Chemistry</p>

**Enhanced Chemotherapeutic Toxicity of Cyclodextrin Templated Size-Tunable
Rhodamine 6G nanoGUMBOS**

Nimisha Bhattarai^a, Mi Chen^a, Rocío L. Pérez^a, Sudhir Ravula^a, Pratap Chhotaray^{a,1},
Suzana Hamdan^{a,2}, Karen McDonough^b, Suman Tiwari^c, and Isiah M. Warner^{*a}

^a Department of Chemistry, Louisiana State University, Baton Rouge, LA 70803, USA.

^b AgCenter Biotechnology Labs, Louisiana State University, Baton Rouge, LA 70803, USA.

^c Department of Biology, University of Louisiana Monroe, Monroe, LA 71209, USA.

¹ Present address – Indian Institute of Technology Delhi, New Delhi, Delhi 110016, India

² Present address – Department of Biochemistry and Molecular Biology, School of Medicine,
University of Miami, Miami, FL 33136, USA.

*Corresponding Author: Isiah M. Warner, email: iwarner@lsu.edu, Phone: 225-578-2829, Fax:
225-578-3458

Abstract:

Nanodrugs have been widely investigated for combating the large number of side effects associated with conventional therapeutics. Several investigations of such nanomedicines have demonstrated the profound role of nanoparticle size in therapeutic efficacy. Herein, we report the role of cyclodextrin (CD)-templating on the size and therapeutic properties of rhodamine 6G (R6G) nanoGUMBOS, i.e. nanomaterials derived from a Group of Uniform Materials Based on Organic Salts (GUMBOS). In these studies, templating of nanoGUMBOS using 2-hydroxypropyl-alpha (2-HP- α), 2-hydroxypropyl beta (2-HP- β), and gamma (γ) cyclodextrin (CD) led to a significant reduction in size and enhanced uniformity as indicated by transmission electron microscopy (TEM) images. In addition, CD-templated nanoGUMBOS remarkably displayed a three to four fold enhancement in toxicity towards cancer cells as compared to nanoGUMBOS without CD-templates, suggesting a significant improvement in therapeutic efficacy. Correlation between size and toxicity suggests that CD-templated nanoparticles of ~70 to 80 nm produced optimal toxicity. Even more interesting, all investigated nanoGUMBOS displayed no toxicity toward normal cells under examined conditions. Moreover, these nanoGUMBOS display comparable chemotherapeutic toxicity to the parent dye, [R6G][Cl], while also eliminating toxicity towards normal cells, indicating their strong chemotherapeutic potential. The studies outlined here provide further insight into an approach that may be employed for rapid synthesis of size tunable nanodrugs for enhanced chemotherapeutic efficacy.

Introduction:

According to the American Cancer Society, cancer was responsible for the death of about 600,000 people in the United States during calendar year 2017.(1) Current chemotherapeutic treatment of cancers suffer from numerous side effects, making development of more selective therapeutics important.(2-4) In this regard, nanomedicines have demonstrated more targeted therapeutic delivery in comparison to conventional chemotherapeutics. Conventional nanomedicines serve as nanocarriers that encapsulate the drug to aid in therapeutic delivery. (5-8)Such nanocarriers are able to provide several advantages for chemotherapeutic drug delivery, including protection of the drug from bio-degradation and rapid permeation into the cell membrane due to nanoscale size.(9-11) Studies of other nanomaterials, derived from transitional metal oxides and sulfides, demonstrate utility for male sterilization and minimization of systemic toxicity.(12, 13) More recent research on nanomedicine focuses on development of nanodrugs fabricated from hydrophobic drugs, such as paclitaxel, in conjunction with a polymeric or inorganic matrix.(14) This approach removes the need for a carrier as the nanoparticle is primarily composed of the drug itself, while the polymeric or inorganic template simply aids in formation of the nanoparticle structure. These nanodrugs have shown promising toxicity *in vitro* and *in vivo* and are also currently being employed in clinical trials.(15)

Our research group has developed highly tunable nanoGUMBOS, i.e nanomaterials derived from a group of uniform materials based on organic salts (GUMBOS). GUMBOS are organic salts typically synthesized using a simple ion-exchange reaction.(16) The variation in counter-ions results in variations in properties, i.e. tunable properties, such as hydrophobicity, conductivity, and melting point, giving these materials a wide variety of applications, including selective chemotherapeutic toxicity.(16, 17) NanoGUMBOS have several distinct advantages over conventional nanomedicines including simple and rapid synthesis, as well as the ability to

serve as the drug rather than the drug carrier. In our previous studies, while we were able to minimize toxicity of the nanoGUMBOS towards normal cells, our nanoGUMBOS displayed a lower chemotherapeutic efficacy as compared to the parent dye.(17) Thus, evaluation of the various factors that affect cytotoxicity may aid in systematic modification of these nanodrugs for improved therapeutic efficacy.

Investigations of various nanoparticles indicate a strong correlation between size, material, hydrophobicity, and surface charge of the nanodrug relative to its toxicity.(18, 19) Size, in particular, was found to play a major role in rapid uptake of nanomaterials into tumor cells. *In vivo* investigations have demonstrated enhanced permeation of the nanomaterials into tumor tissues due to leaky tumor vasculature through a phenomenon known as enhanced permeability and retention (EPR) effect.(20-22) Additionally, *in vitro* investigations have demonstrated that nanoparticles typically internalize using various size dependent active transport pathways. (23-26) In this regard, several investigations have demonstrated that tuning the size of nanoparticles to around 100 nm leads to enhanced endocytic uptake which can ultimately affect the toxicity of these materials. Thus, it becomes essential to develop an approach to rapidly tune size and uniformity of the nanomaterial in order to optimize toxicity. However, a major challenge associated with controlled size of current nanodrugs, that employ polymeric and inorganic materials, is the complex and labor intensive synthetic route typically associated with such approaches.(27)

Cyclodextrins (CDs) have been employed as templates for nanoparticle synthesis to control both nanoparticle size and uniformity.(28) CDs are oligosaccharides that can typically be used for hydrophobic drug encapsulation in order to enhance solubility.(29-31) These oligosacchariodes are typically divided into three classes (α -CD, β -CD, and γ -CD) that vary in

cavity sizes, with γ -CD being the largest and α -CD being the smallest.(32) This varying cavity size allows for optimization of interactions between drug and CD. For example, drug molecules with large aromatic rings are more likely to be encapsulated using β or γ -CD than α -CD.(33) Recent studies have shown that the hollow, and hydrophobic cavity of cyclodextrin can also serve as a template to control size and uniformity of nanoparticles.(28, 34-36) Specifically, studies by Hamdan et al. have revealed that use of cyclodextrin to template nanoGUMBOS produced smaller, more uniform, and more potent nanomaterials.(28) In contrast to conventional polymer and inorganic materials currently being employed for nanodrug fabrication, the relatively higher water solubility of CD also improves therapeutic delivery.(32)

In the studies presented here, we examine the influence of 2-hydroxypropyl-alpha (2-HP- α -CD), 2-hydroxypropyl-beta (2-HP- β -CD), and gamma (γ -CD) templates on the size, uniformity and therapeutic properties of nanoGUMBOS derived from rhodamine 6G (R6G), a fluorescent mitochondrial toxin known to have promising anticancer properties.(37) Following synthesis, these nanomaterials were characterized using transmission electron microscopy (TEM), dynamic light scattering (DLS) and zeta potential. Subsequently, the cytotoxicities of these nanodrugs were evaluated using MDA-MB-231 breast cancer and Hs578Bst normal breast cells. Cytotoxicity was then correlated to the cellular uptake and size to provide further understanding of the therapeutic properties of these nanodrugs. Additionally, subcellular localization was also investigated to assess variations in mitochondrial localization following CD-templating.

Materials and Methods:

Materials: Rhodamine 6G (95%), phosphate buffered saline (10x concentrate, 0.2 μ M filtered), sodium tetrphenylborate [Na][TPB], methylene chloride, dimethylsulfoxide, citric acid

monohydrate, 2HP- α -CD, 2HP- β -CD, human serum and 0.2 μ M nylon filters were purchased from Sigma-Aldrich (Milwaukee, WI). Gamma-CD (γ -CD) was purchased from Fluka (Germany). Sodium phosphate dibasic was purchased from Fisher Scientific (Fair Lawn, New Jersey). Lithium bis (perfluoroethylsulfonyl) imide [Li][BETI] was obtained from Ionic Liquid Technologies (Tuscaloosa, Al). Triply deionized water was obtained using an Aires High Purity Water System (Port Allen, LA). The cell viability MTT (3-[4, 5-Dimethylthiazol-2-yl]-2, 5-diphenyltetrazolium bromide) assay was purchased from Promega Corporation (Madison, WI). TEM grids were purchased from Ted Pella (Redding, CA).

Synthesis of nanoGUMBOS: NanoGUMBOS were synthesized using a modified protocol obtained from literature.(28) Briefly, a 1 mM solution of [R6G][Cl] with and without cyclodextrin (0.8 mg) was mixed with a 1 mM solution of [Li][BETI] or [Na][TPB]. An ultrasonic processor was used to probe sonicate this solution in an ice bath at 20% amplitude and 30 mHz for 5 minutes. Each sample was then centrifuged twice at 35,000 rpm for 30 minutes using a Beckman L8-70M Ultracentrifuge and the pellet was washed several times with water to remove excess cyclodextrin and LiCl byproduct. Finally, the product was dried by removal of water *in vacuo* using a Labconco freeze dry system. All nanoGUMBOS were resuspended with bath ultrasonication for 2 h in cell media to ensure homogeneity prior to cell studies.

Dynamic Light Scattering and Zeta Potential: NanoGUMBOS were resuspended in 0.01 M PBS buffer to produce a 100 μ M solution. These nanoGUMBOS were then diluted to 5 μ M for DLS and zeta potential measurements.

Spectral Studies: NanoGUMBOS were resuspended in 0.01 M PBS buffer to create a 100 μ M solution. These nanoGUMBOS were diluted to 1 μ M for spectral measurements. Absorbance measurements were performed using a Shimadzu UV-3101PC UV-Vis

Spectrophotometer. Samples for fluorescence measurements were excited at the absorbance λ_{\max} using a HORRIBA fluorimeter to obtain the reported spectrum.

Serum Stability: The absorbance of a 1 μM in PBS buffer containing 10% serum was monitored for 48 h using a Shimadzu UV-3101PC UV-Vis Spectrophotometer.

Cell Culture: MDA-MB-231 breast adenocarcinoma cells, Mia-Paca pancreatic carcinoma and Hs578Bst normal breast fibroblast cells were purchased from the American Tissue Culture Collection (ATCC, Manassas, VA). All cell lines were grown to 90% confluency according to the ATCC guidelines prior to plating.

Cytotoxicity Studies: A 96 well plate was seeded with 5000 cells/well and incubated for 24 h to allow the cells to attach. Cells were treated with a serial dilution of nanoGUMBOS and the last row was kept as an untreated control using only cell media. An MTT assay was then performed to determine cell viability. In brief, cells were treated with 15 μL of MTT assay and incubated for 3 h. Then, 100 μL of stop solution was added to solubilize the purple formazan crystals. A microplate spectrophotometer was used to measure the absorbance at 570 nm. Cell viability was calculated as a percentage of the ratio between absorbance of treated cells and absorbance of the control containing only cell media. All measurements were performed in triplicate and reported cell viabilities represent an average of these measurements.

Cellular Uptake Studies: The cellular uptake studies were performed in triplicate using 35 mM petri dishes plated with 200,000 cells/dish for 24 hrs. These cells were treated with a 5 μM nanoGUMBOS solution and incubated at 37°C for 5 hrs. The control sample was only incubated with fresh cell media without nanoGUMBOS. After 5 h incubation, it was assumed that some of the nanoparticles had internalized. Cells were then washed with PBS buffer several times to remove excess compound that was not internalized. Cells were then treated with 3 mL

of DMSO for 5 h in order to lyse the cells and release any internalized drug. Subsequently, the absorbance of the DMSO solutions was examined using a Shimadzu UV-3101PC UV-Vis Spectrophotometer. All measurements were performed using control cells treated with only cell media as the reference. A set of five DMSO calibration standards from 1-10 μM , were prepared in triplicate for each nanoGUMBOS, and the absorbance of each solution was recorded. The internalized concentration of nanoGUMBOS present in the DMSO of treated cells was calculated through use of a calibration curve generated from these standards.

Fluorescence Microscopy: Briefly, 100,000 MDA-MB-231 breast cancer cells were seeded in 35 mm petri dishes (10 mm micro cell; Ashland, MA, USA) in 3 mL of cell media and incubated at 37 °C for 24 h. Cells were then treated with 10 nM mitotracker for 20 minutes at 37 °C. Subsequently, cells were washed with PBS and then treated with 25 nM of nanoGUMBOS for 30 minutes. Cells were then washed again with PBS buffer prior to imaging with a fluorescence microscope (Leica, TCS SP5, Mannheim, Germany) using a 40X dipping objective.

Results and Discussion

Characterization of nanoGUMBOS: R6G nanoGUMBOS were synthesized via an ultrasonication assisted ion exchange reaction between [R6G][Cl] and lithium bis (perfluoroethylsulfonyl)imide [Li][BETI] or sodium tetraphenylborate [Na][TPB] to respectively form [R6G][BETI] and [R6G][TPB] nanoGUMBOS in presence and absence of a CD-template. This ion-exchange reaction is depicted in supplemental Figure S1. As indicated by Hamdan, et al., variations in reactant concentration leads to a negligible effect on particle size in the presence of a 2-HP- β -CD template; thus, we employed CDs with varying cavity sizes to optimize size of the nanoGUMBOS.⁽²⁸⁾ For all CD-templated nanoGUMBOS, we maintain a 1:1 ratio between

CD template and reactants due to the known renal toxicity of CD with *in vivo* and clinical applications.(29)

Synthesized nanoGUMBOS were characterized using several analytical techniques including mass spectrometry, Fourier-transform infrared spectroscopy (FTIR), and nuclear magnetic resonance (NMR). The presence of [BETI] and [TPB] counter-ion peaks in the negative ion mode electrospray ionization mass spectrum indicates successful ion exchange of [R6G][Cl] to form respective nanoGUMBOS (supplemental Figures S2 and S3). FTIR and NMR of [R6G][BETI] and [R6G][TPB] display no peak shifts for the CD-templated nanoGUMBOS (Supplemental Figures S4 and S5). In addition, the absence of CD peaks in both FTIR and NMR spectra further confirms that CD was only used as a template and appears to be washed away after formation of products. Lastly, the absence of CD peaks in MALDI mass spectrum (Supplemental Figures S6-S9) provides further confirmation that CD primarily serves as a template and is removed during the synthesis.

Following synthesis, size and shape of the nanoGUMBOS were characterized using TEM microscopy. Figure 1a and 1b portray TEM images of respectively [R6G][TPB] and [R6G][BETI] nanoGUMBOS with and without CD-templating. As indicated by examination of the TEM images, quasi-spherical nanoGUMBOS were formed for both [R6G][TPB] and [R6G][BETI] nanoGUMBOS. Table 1 is a summary of sizes for both [R6G][TPB] and [R6G][BETI] nanoGUMBOS synthesized with and without the CD-template. Reported sizes represent the average of the sizes measured for 200 representative nanoparticles for each image along with their respective standard deviations. As reported in table 1, a significant reduction in size was observed with CD-templating for both [R6G][TPB] and [R6G][BETI] nanoGUMBOS. In this regard, while the [R6G][TPB] nanoGUMBOS without a CD-template displayed a size of

~ 100 nm, this size was reduced to 50-70 nm for the CD-templated nanoGUMBOS. Similarly, [R6G][BETI] nanoGUMBOS without a CD-template displayed a size of ~ 100 nm, and this size was reduced to 70-80 nm for the CD-templated nanoGUMBOS. Additionally, both [R6G][TPB] and [R6G][BETI] CD-templated nanoGUMBOS displayed improved uniformity as compared to respective controls.

Interestingly, examination of results from this TEM analysis suggests that size of the nanoparticle depends primarily upon both the reactant structure and the CD cavity. As reported in Table 1, a 50% reduction in nanoparticle size was observed for 2HP- α -CD, and 2HP- β -CD [R6G][TPB] nanoGUMBOS while a larger size was observed for γ -CD [R6G][TPB]. This difference in size can be attributed to the relatively smaller cavity size of the alpha and beta CD as compared to gamma CD.(38) In contrast, while a slight variation in size was observed, all [R6G][BETI] CD-templated nanoGUMBOS had relatively similar sizes. This narrow range is likely due to the smaller aliphatic structure of [BETI]⁻ as compared to the bulky aromatic structure of [TPB]⁻. In this regard, a larger cavity size is more likely to optimally fit the larger aromatic ring structure of TPB, resulting in larger variations in size.(32) Overall, the observed reduction in size (44-89 nm) and improved uniformity of nanoGUMBOS templated with CD, as compared to their respective controls, coincides well with the conclusions by Hamdan et al., and also suggests that such nanoparticles may result in enhanced cellular uptake and thus enhanced therapeutic properties.(28)

DLS and zeta potential measurements were performed to further understand the effect of cyclodextrin on size distribution and stability of the nanoGUMBOS. Examination of DLS measurements indicated that all synthesized nanoGUMBOS displayed a polydispersity of ~0.2; thus, indicating relatively monodispersed nanoparticles. These data are consistent with the

uniform nanoparticles observed for TEM analysis of CD-templated nanoGUMBOS, further corroborating our findings. Zeta potential measurements were performed in phosphate buffered saline at physiological pH (pH 7.4) in order to mimic a respective biological environment. As shown in table 1, while the zeta potential measurement for [R6G][TPB] is around -23 mV, CD-templated nanoGUMBOS displayed a zeta potential of around -28 mV indicating formation of slightly more stable nanoparticles with cyclodextrin template. Similar results were observed for [R6G][BETI] nanoGUMBOS where the zeta potential varied from around approximately -24 mV to -29 mV for the control and CD-templated nanoGUMBOS respectively. These results indicate that use of CD-templating led to improved stability of R6G-based nanoGUMBOS.

Subsequently, spectral properties of nanoGUMBOS in PBS buffer were also assessed to evaluate any variation in photo-physical properties with CD-templating. As shown in supplemental Figures S10 and S11, both [R6G][TPB] and [R6G][BETI] nanoGUMBOS display an absorbance and emission peak maxima of approximately 520 and 550 nm, which corresponds to the absorbance and emission wavelengths of the parent dye [R6G][Cl].⁽¹⁷⁾ All CD-templated nanoGUMBOS displayed a slight 5-10 nm blue shift in absorbance and fluorescence emission as compared to the respective controls without CD-template. This shift could possibly be due to H-type aggregation resulting from face to face molecular arrangement.⁽³⁹⁾ All nanoGUMBOS displayed strong fluorescence emissions in PBS buffer suggesting their potential to serve as a biomedical imaging agents in addition to their therapeutic applications. As most *in vivo* investigations are performed in PBS in contrast to cell medium, evaluation of the stability of these nanomaterials in PBS is essential. As shown in Figure 2, these nanoGUMBOS demonstrate favorable stability in PBS supplemented with 10% FBS, indicating their potential *in vivo*

applications. These results are consistent with our previous studies that demonstrate favorable stability of R6G nanoGUMBOS in 10% serum solution.(17)

Examination of Cell Viability: Following detailed characterization, nanoGUMBOS were then employed *in vitro* to assess the effect of this size variation on cytotoxicity. Figure 3 is a graphical representation of the cytotoxicity of [R6G][TPB] nanoGUMBOS with and without CD templating towards MDA-MB-231 breast cancer cells. The IC_{50} values, i.e. the concentration at which 50% inhibition of cell growth occurs, for [R6G][TPB] nanoGUMBOS are reported in Table 2. Interestingly, an enhanced cytotoxicity was observed for CD-templated [R6G][TPB] nanoGUMBOS as compared to the nanoGUMBOS alone. In this regard, while the [R6G][TPB] nanoGUMBOS without CD template displayed an IC_{50} value of 7.3 $\mu\text{g/mL}$, templating with 2HP- α and 2HP- β -CD led to a three-fold reduction in IC_{50} value to 2.6 $\mu\text{g/mL}$ and 2.7 $\mu\text{g/mL}$ respectively. In contrast, templating with γ -CD led to a five-fold reduction in the IC_{50} to 1.44 $\mu\text{g/mL}$. By use of statistical analysis, we concluded that the IC_{50} concentration of [R6G][TPB] nanoGUMBOS templated with γ -CD was significantly different from those templated with 2HP- α and 2HP- β -CD with a 95% confidence level.

Dose dependent cytotoxicity of the [R6G][BETI] nanoGUMBOS with and without cyclodextrin templating is presented in Figure 4. Similar to the [R6G][TPB] nanoGUMBOS, an enhanced cytotoxicity was observed for CD-templated [R6G][BETI] nanoGUMBOS as compared to nanoparticles alone. In this regard, CD-templating led to a decrease in IC_{50} concentration from 4.2 $\mu\text{g/mL}$ for nanoGUMBOS alone to 2.3 $\mu\text{g/mL}$ for the γ -CD templated nanoGUMBOS, suggesting a two-fold increase in toxicity. Templating with 2HP- α and 2HP- β -CD led to an even greater reduction in IC_{50} concentration to 1.6 $\mu\text{g/mL}$ and 1.7 $\mu\text{g/mL}$, respectively. Statistical analysis of these means, however, suggested that the variations in IC_{50}

concentration with CD-cavity size were not significantly different. This indicates that, in contrast to CD-templated [R6G][TPB] nanoGUMBOS, toxicity of CD-templated [R6G][BETI] nanoGUMBOS was independent of CD-cavity size. Evaluation of the toxicity of the parent dye, [R6G][Cl], with respect to the MDA-MB-231 breast cancer cells revealed an IC_{50} concentration of 2.8 $\mu\text{g/mL}$, which is consistent with previous literature.⁽¹⁷⁾ It is interesting to note that while nanoGUMBOS without CD template displayed lower toxicity than the parent dye towards MDA-MB-231 breast cancer cells, CD-templated nanoGUMBOS displayed a comparable toxicity.

Correlation between size and cytotoxicity of [R6G][TPB] CD-templated nanoGUMBOS indicates an optimal size for enhanced toxicity. In this regard, γ -CD templated [R6G][TPB] nanoparticles have a size of ~ 70 nm, while 2HP- β -CD and 2HP- α -CD templated [R6G][TPB] nanoparticles display sizes below 60 nm. Comparison of their IC_{50} values indicates that γ -CD templated nanoparticles displayed a 50% reduction in IC_{50} concentration as compared to 2HP- β -CD and 2HP- α -CD templated nanoparticles. Moreover, this suggests that 70 nm nanoparticles obtained using γ -CD templating led to optimal toxicity for the [R6G][TPB] nanoGUMBOS. Similar to the [R6G][TPB] nanoGUMBOS, CD-templated [R6G][BETI] nanoGUMBOS also displayed a significant reduction in IC_{50} concentration; however, this reduction was independent of CD cavity size. In this regard, all IC_{50} concentrations for CD-templated [R6G][BETI] nanoGUMBOS were relatively similar. This minimal difference in IC_{50} concentration can be attributed to the relatively similar size of these nanoGUMBOS (~ 70 -80 nm). Furthermore, optimal toxicity for [R6G][TPB] nanoGUMBOS obtained from 70 nm γ -CD templated nanoGUMBOS, is relatively similar to that of all CD-templated [R6G][BETI] nanoGUMBOS (~ 70 -80 nm). This indicates that 70-80 nm is most probably an optimal size for improved toxicity of nanoGUMBOS developed from R6G.

Toxicity of the nanoGUMBOS was then assessed in Mia-Paca pancreatic cancer cells in order to further corroborate our results. Remarkably, all synthesized nanoGUMBOS displayed less than 1 $\mu\text{g/mL}$ IC_{50} values toward Mia-Paca pancreatic cancer cells, suggesting their strong therapeutic potential towards this cell line. Similar to their behavior in MDA-MB-231 breast cancer cells, all CD-templated [R6G][TPB] and [R6G][BETI] nanoGUMBOS displayed improved therapeutic efficacy towards Mia-Paca pancreatic cancer cells as compared to the respective controls without CD template (Table 2). [R6G][TPB] nanoGUMBOS templated with γ -CD displayed a statistically significant decrease in IC_{50} concentration as compared to nanoGUMBOS templated with 2HP- α CD and 2HP- β -CD. In contrast, all CD-templated [R6G][BETI] nanoGUMBOS displayed relatively similar IC_{50} values. Moreover, these results are consistent with our findings for the MDA-MB-231 breast cancer cells. Thus, from these studies we conclude that while toxicity of the CD-templated [R6G][TPB] nanoGUMBOS varies with CD cavity size, the toxicity of the CD-templated [R6G][BETI] nanoGUMBOS is not affected by variations in CD.

Cellular uptake and subcellular localization of nanoGUMBOS: In order to further understand the relationship between reduced nanoparticle size and enhanced toxicity of the nanoGUMBOS, cellular uptake was examined. Figures 5a, and 5b display the cellular uptake (nmol) of 5 μM [R6G][TPB] and [R6G][BETI] nanoGUMBOS respectively after 5 h in MDA-MB-231 breast cancer cells. As shown in Figure 5a, significantly enhanced cellular uptake was observed for [R6G][TPB] and [R6G][BETI] CD templated nanoGUMBOS as compared to the respective nanoGUMBOS without CD. This enhanced cellular uptake of CD-templated nanoGUMBOS is consistent with the observed enhanced cytotoxicity of these materials.

Furthermore this enhancement is likely a combination of the reduced size, improved uniformity, and enhanced stability of the CD-templated nanoGUMBOS.

Comparison between different types of CDs indicates that [R6G][TPB] nanoGUMBOS templated with 2HP- β -CD display a relatively lower cellular uptake as compared to nanoGUMBOS templated with 2HP- α -CD or γ -CD. In this regard, the relatively smaller size of β -CD templated [R6G][TPB] nanoGUMBOS may allow for rapid internalization and excretion of these materials leading to poor cellular retention.⁽⁴⁰⁾ Additionally, while 2HP- α -CD templated [R6G][TPB] nanoGUMBOS display comparable cellular uptake to γ -CD templated [R6G][TPB] nanoGUMBOS, they display a statistically significant reduction in toxicity. This behavior can be attributed to the \sim 50 nm size of these nanoGUMBOS since literature suggests poor cellular retention for nanoparticles less than 50 nm after 24 h.⁽⁴¹⁾ In this regard, while a relatively high cellular uptake is observed after 5 h, this poor cellular retention may have affected the toxicity which is measured after 48 h. All CD-templated [R6G][BETI] nanoGUMBOS with similar sizes (70-80 nm) displayed similar cellular uptakes, which is consistent with their relatively similar IC_{50} concentrations. Moreover, from these results, we can conclude a strong correlation between size, toxicity, and cellular uptake of nanoGUMBOS. Thus, our studies demonstrate that cyclodextrin templating leads to reduced size, enhanced cellular uptake and improved cytotoxicity of R6G nanoGUMBOS. This observation is consistent with several studies which have found that reduced size results in increased cellular uptake due to the EPR effect and variations in internalization pathways.⁽⁴²⁾⁽⁴³⁾

Following evaluation of cellular uptake, subcellular localization of the nanoGUMBOS in MDA-MB-231 breast cancer cells was assessed using fluorescence microscopy. As previous literature has shown that the parent dye, [R6G][Cl], is a known mitochondrial toxin,

understanding the effect of CD-templating on the mitochondrial localization may aid to further elucidate their therapeutic behavior.⁽¹⁷⁾ Evaluation of microscopy images displayed in Figure S12 and colocalization coefficients presented in table S1 suggest complete co-localization of the Mitotracker green dye with the R6G nanoGUMBOS. Thus, from these results we conclude that subcellular localization of these nanoGUMBOS was unaffected by CD-templating. Moreover, since all nanoGUMBOS display similar intracellular accumulation behaviors, the observed reduction in IC_{50} for the CD-templated nanoGUMBOS can primarily be attributed to reduced size and improved uniformity of these materials.

Examination of Selectivity: After detailed understanding of nanoGUMBOS behavior in cancer cells, toxicities were examined using Hs578Bst normal breast cells in order to investigate the effect of cyclodextrin on the selective toxicity of these nanomaterials. Figure 6 is a graphical representation of the toxicity of [R6G][TPB] and [R6G][BETI] with and without cyclodextrin templating towards Hs578Bst normal breast cells. Intriguingly, as seen in Figure 6, the cell viability was essentially 100% for both [R6G][TPB] and [R6G][BETI] CD-templated nanoGUMBOS, which is similar to the respective controls without CD. This indicates that while CD templating enhances the toxicity of the nanomaterials towards cancer cells, the nontoxic behavior in normal cells remains unaffected under experimental conditions.

Examination of the toxicity of the parent dye [R6G][CI] revealed an IC_{50} of $\sim 2.3 \mu\text{g/mL}$ and $\sim 16 \mu\text{g/mL}$ towards MDA-MB-231 breast cancer cells and Hs578Bst normal cells respectively. Thus, from these results we conclude that CD-templated [R6G][TPB] and [R6G][BETI] nanoGUMBOS display comparable therapeutic properties to [R6G][CI], while minimizing the toxicity towards normal cells. In contrast to conventional chemotherapeutic agents such as Paclitaxel and Gemcitabine, our nanoGUMBOS display a slightly higher IC_{50}

towards MDA-MB-231 breast cancer cells.(44) However, the nontoxic behavior of our nanoGUMBOS towards Hs578Bst normal cells suggests that employing this therapeutic approach may lead to reduction of the toxic effects associated with these current therapeutics.(44) Remarkably, in the case of the MiaPaca-2 pancreatic cancer cells, our nanoGUMBOS demonstrate comparable therapeutic efficacy to these Gemcitabine, a known chemotherapeutic agent commonly employed to treat pancreatic cancer.(45) Thus, further investigation of pancreatic cell lines may provide further insight to the therapeutic application of these nanoGUMBOS. Overall, these results demonstrate the strong therapeutic potential of these nanoGUMBOS for favorable *in vivo* applications.

Conclusion

The studies reported here suggest a simple and rapid synthesis technique for controlling size and ultimately tuning the cytotoxicity of nanodrugs. These studies demonstrate that CD-templated nanoparticles display reduced size and improved stability that provides several benefits for use in biological systems. Significantly improved *in vitro* toxicity was observed for [R6G][BETI] and [R6G][TPB] CD-templated nanoGUMBOS as compared to a control without CD. Furthermore, γ -CD-templated [R6G][TPB] nanoGUMBOS displayed enhanced toxicity towards MDA-MB-231 breast cancer cells as compared to 2HP- β and 2HP- α -CD templated nanoGUMBOS. In contrast, the IC_{50} concentration was relatively similar among the CD-templated [R6G][BETI] nanoGUMBOS. Moreover, 70 nm γ -CD [R6G][TPB] nanoGUMBOS and ~70-80 nm R6G BETI CD-templated nanoGUMBOS displayed similar IC_{50} concentrations. Thus, from these results, we conclude that 70-80 nm particles displayed optimal *in vitro* therapeutic properties for nanoGUMBOS derived from R6G. Further examination of these nanoGUMBOS indicates no toxicity toward normal breast cells under reported conditions.

Moreover, these studies are a report of the effect of reduced size on the toxicity of rhodamine 6G nanoGUMBOS and these results provide possible insights into use of similar strategies for other chemotherapeutic nanodrugs.

Acknowledgements

This material is based upon work supported in part by the National Science Foundation under Grant No. CHE-1508726. Any opinions, findings, and conclusions or recommendations expressed in this material are those of the author(s) and do not necessarily reflect the views of the National Science Foundation. The use of the LSU Shared Instrumentation Facility is also acknowledged.

Conflict of Interest

The authors declare no potential conflicts of interest.

References

1. Society AC. Cancer Facts and Figures 2017 2017 [Available from: www.cancer.org.
2. Miller KD, Siegel RL, Lin CC, Mariotto AB, Kramer JL, Rowland JH, et al. Cancer treatment and survivorship statistics, 2016. *CA: a cancer journal for clinicians*. 2016;66(4):271-89.
3. Park K. Facing the truth about nanotechnology in drug delivery. *ACS Nano*. 2013;7(9):7442-7.
4. Chen Z, Li B, Xie X, Zeng F, Wu S. A sequential enzyme-activated and light-triggered pro-prodrug nanosystem for cancer detection and therapy. *Journal of Materials Chemistry B*. 2018.
5. Wicki A, Witzigmann D, Balasubramanian V, Huwyler J. Nanomedicine in cancer therapy: Challenges, opportunities, and clinical applications. *Journal of Controlled Release*. 2015;200:138-57.
6. Krishnamurthy S, Vaiyapuri R, Zhang L, Chan JM. Lipid-coated polymeric nanoparticles for cancer drug delivery. *Biomaterials Science*. 2015;3(7):923-36.
7. Mura S, Nicolas J, Couvreur P. Stimuli-responsive nanocarriers for drug delivery. *Nature materials*. 2013;12(11):991-1003.
8. Liu Z, Huang Y, Pu F, Ren J, Qu X. Conformational switch-mediated accelerated release of drug from cytosine-rich nucleic acid-capped magnetic nanovehicles. *Chemical Communications*. 2016;52(16):3364-7.
9. Markman JL, Rekechenetskiy A, Holler E, Ljubimova JY. Nanomedicine therapeutic approaches to overcome cancer drug resistance. *Advanced Drug Delivery Reviews*. 2013;65(13-14):1866-79.
10. Kumari A, Yadav SK, Yadav SC. Biodegradable polymeric nanoparticles based drug delivery systems. *Colloids and Surfaces B: Biointerfaces*. 2010;75(1):1-18.
11. Albanese A, Tang PS, Chan WC. The effect of nanoparticle size, shape, and surface chemistry on biological systems. *Annual review of biomedical engineering*. 2012;14:1-16.
12. Liu Z, Liu X, Du Y, Ren J, Qu X. Using Plasmonic Copper Sulfide Nanocrystals as Smart Light-Driven Sterilants. *ACS Nano*. 2015;9(10):10335-46.
13. Liu Z, Liu X, Ran X, Ju E, Ren J, Qu X. Single-layer tungsten oxide as intelligent photo-responsive nanoagents for permanent male sterilization. *Biomaterials*. 2015;69:56-64.
14. D'Addio SM, Prud'homme RK. Controlling drug nanoparticle formation by rapid precipitation. *Advanced Drug Delivery Reviews*. 2011;63(6):417-26.
15. Junghanns J-UAH, Müller RH. Nanocrystal technology, drug delivery and clinical applications. *International Journal of Nanomedicine*. 2008;3(3):295-310.
16. Warner IM, El-Zahab B, Siraj N. Perspectives on Moving Ionic Liquid Chemistry into the Solid Phase. *Analytical Chemistry*. 2014;86(15):7184-91.
17. Magut PKS, Das S, Fernand VE, Losso J, McDonough K, Naylor BM, et al. Tunable Cytotoxicity of Rhodamine 6G via Anion Variations. *Journal of the American Chemical Society*. 2013;135(42):15873-9.
18. Greish K. Enhanced permeability and retention of macromolecular drugs in solid tumors: a royal gate for targeted anticancer nanomedicines. *Journal of drug targeting*. 2007;15(7-8):457-64.
19. Lee S-J, Jeong Y-IL. Hybrid nanoparticles based on chlorin e6-conjugated hyaluronic acid/poly(l-histidine) copolymer for theranostic application to tumors. *Journal of Materials Chemistry B*. 2018.
20. Jain RK, Stylianopoulos T. Delivering nanomedicine to solid tumors. *Nature reviews Clinical oncology*. 2010;7(11):653-64.

21. Peer D, Karp JM, Hong S, Farokhzad OC, Margalit R, Langer R. Nanocarriers as an emerging platform for cancer therapy. *Nat Nano*. 2007;2(12):751-60.
22. Greish K. Enhanced permeability and retention (EPR) effect for anticancer nanomedicine drug targeting. In: Grobmyer SR, Moudgil BM, editors. *Cancer Nanotechnology: Methods and Protocols*. Totowa, NJ: Humana Press; 2010. p. 25-37.
23. Tang L, Yang X, Yin Q, Cai K, Wang H, Chaudhury I, et al. Investigating the optimal size of anticancer nanomedicine. *Proceedings of the National Academy of Sciences*. 2014;111(43):15344-9.
24. Maeda H, Nakamura H, Fang J. The EPR effect for macromolecular drug delivery to solid tumors: Improvement of tumor uptake, lowering of systemic toxicity, and distinct tumor imaging in vivo. *Advanced Drug Delivery Reviews*. 2013;65(1):71-9.
25. Blanco E, Shen H, Ferrari M. Principles of nanoparticle design for overcoming biological barriers to drug delivery. *Nat Biotech*. 2015;33(9):941-51.
26. Torchilin V. Tumor delivery of macromolecular drugs based on the EPR effect. *Advanced Drug Delivery Reviews*. 2011;63(3):131-5.
27. Farokhzad OC, Langer R. Nanomedicine: Developing smarter therapeutic and diagnostic modalities. *Advanced Drug Delivery Reviews*. 2006;58(14):1456-9.
28. Hamdan S, Dumke JC, El-Zahab B, Das S, Boldor D, Baker GA, et al. Strategies for controlled synthesis of nanoparticles derived from a group of uniform materials based on organic salts. *Journal of Colloid and Interface Science*. 2015;446:163-9.
29. Tiwari G, Tiwari R, Rai AK. Cyclodextrins in delivery systems: Applications. *Journal of Pharmacy and Bioallied Sciences*. 2010;2(2):72-9.
30. Zhang J, Ma PX. Cyclodextrin-based supramolecular systems for drug delivery: Recent progress and future perspective. *Advanced Drug Delivery Reviews*. 2013;65(9):1215-33.
31. Brewster ME, Loftsson T. Cyclodextrins as pharmaceutical solubilizers. *Advanced Drug Delivery Reviews*. 2007;59(7):645-66.
32. Davis ME, Brewster ME. Cyclodextrin-based pharmaceuticals: past, present and future. *Nature Reviews Drug Discovery*. 2004;3(12):1023-35.
33. Del Valle EM. Cyclodextrins and their uses: a review. *Process biochemistry*. 2004;39(9):1033-46.
34. Bleta R, Lannoy A, Machut C, Monflier E, Ponchel A. Understanding the Role of Cyclodextrins in the Self-Assembly, Crystallinity, and Porosity of Titania Nanostructures. *Langmuir*. 2014;30(39):11812-22.
35. Chung JW, Guo Y, Kwak S-Y, Priestley RD. Understanding and controlling gold nanoparticle formation from a robust self-assembled cyclodextrin solid template. *Journal of Materials Chemistry*. 2012;22(13):6017-26.
36. Ganguly BN, Verma V, Chatterjee D, Satpati B, Debnath S, Saha P. Study of gallium oxide nanoparticles conjugated with β -cyclodextrin: an application to combat cancer. *ACS Applied Materials & Interfaces*. 2016;8(27):17127-37.
37. Kutushov M, Gorelik O. Low concentrations of Rhodamine-6G selectively destroy tumor cells and improve survival of melanoma transplanted mice. *Neoplasma*. 2013;60(3):262-73.
38. van de Manacker F, Vermonden T, van Nostrum CF, Hennink WE. Cyclodextrin-based polymeric materials: synthesis, properties, and pharmaceutical/biomedical applications. *Biomacromolecules*. 2009;10(12):3157-75.
39. Más-Montoya M, Janssen RAJ. The effect of H- and J-aggregation on the photophysical and photovoltaic properties of small thiophene-pyridine-DPP molecules for bulk-heterojunction solar cells. *Advanced Functional Materials*. 2017;27(16):1605779.
40. Li S-D, Huang L. Pharmacokinetics and biodistribution of nanoparticles. *Molecular pharmaceuticals*. 2008;5(4):496-504.

41. Liu X, Chen Y, Li H, Huang N, Jin Q, Ren K, et al. Enhanced retention and cellular uptake of nanoparticles in tumors by controlling their aggregation behavior. *ACS Nano*. 2013;7(7):6244-57.
42. Acharya S, Sahoo SK. PLGA nanoparticles containing various anticancer agents and tumour delivery by EPR effect. *Advanced Drug Delivery Reviews*. 2011;63(3):170-83.
43. Svenson S, Prud'homme RK. Multifunctional nanoparticles for drug delivery applications: imaging, targeting, and delivery: Springer Science & Business Media; 2012.
44. Liu K, Cang S, Ma Y, Chiao JW. Synergistic effect of paclitaxel and epigenetic agent phenethyl isothiocyanate on growth inhibition, cell cycle arrest and apoptosis in breast cancer cells. *Cancer Cell International*. 2013;13(1):10.
45. Awasthi N, Zhang C, Schwarz AM, Hinz S, Wang C, Williams NS, et al. Comparative benefits of Nab-paclitaxel over gemcitabine or polysorbate-based docetaxel in experimental pancreatic cancer. *Carcinogenesis*. 2013;34(10):2361-9.

Figures and Figure Legends

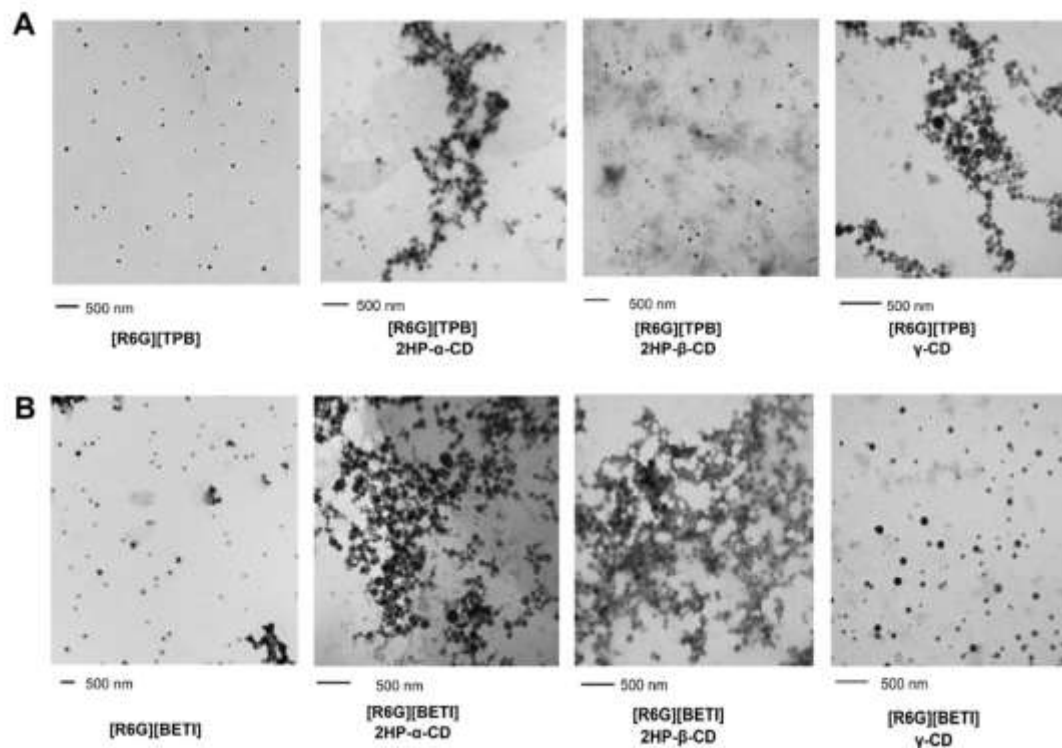


Figure 1. TEM images of 100 μ M (A) [R6G][TPB] and (B) [R6G][BETI] nanoGUMBOS with and without cyclodextrin

Table 1. Sizes and Zeta Potential of [R6G][TPB] and [R6G][BETI] nanoGUMBOS

NanoGUMBOS	Size	Zeta Potential
[R6G][TPB] Control	105 \pm 16 nm	-23.1 \pm 1.2 mV
[R6G][TPB] 2HP- α -CD	55 \pm 6 nm	-27.2 \pm 1.5 mV
[R6G][TPB] 2HP- β -CD	44 \pm 4 nm	-29.5 \pm 1.1 mV
[R6G][TPB] γ -CD	69 \pm 6 nm	-28.3 \pm 0.9 mV
[R6G][BETI] Control	99 \pm 12 nm	-24.3 \pm 1.2 mV
[R6G][BETI] 2HP- α -CD	68 \pm 8 nm	-29.0 \pm 1.1 mV
[R6G][BETI] 2HP- β -CD	66 \pm 4 nm	-30.1 \pm 0.8 mV
[R6G][BETI] γ -CD	80 \pm 5 nm	-29.8 \pm 1.6 mV

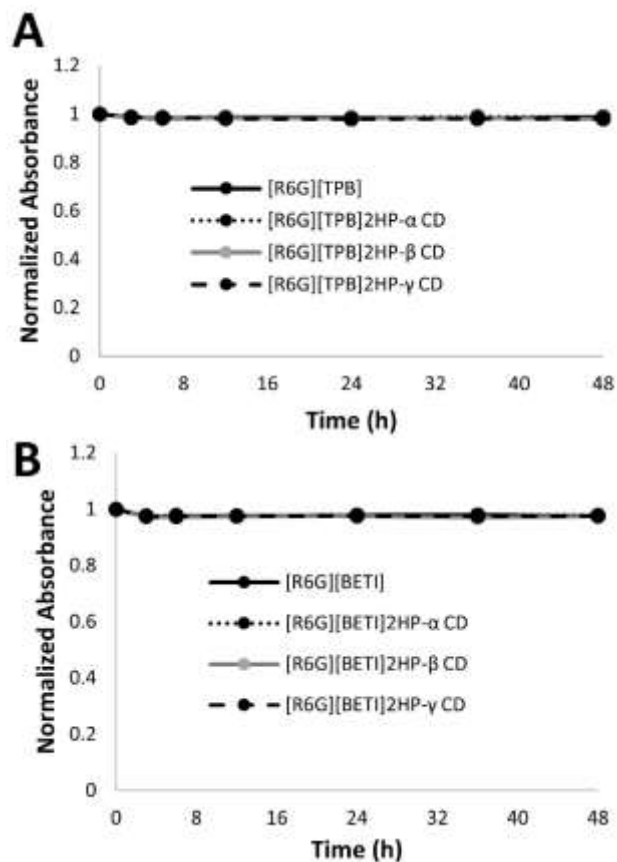


Figure 2. Stability of (A) [R6G][TPB] and (B) [R6G][BETI] nanoGUMBOS in PBS buffer containing 10% serum

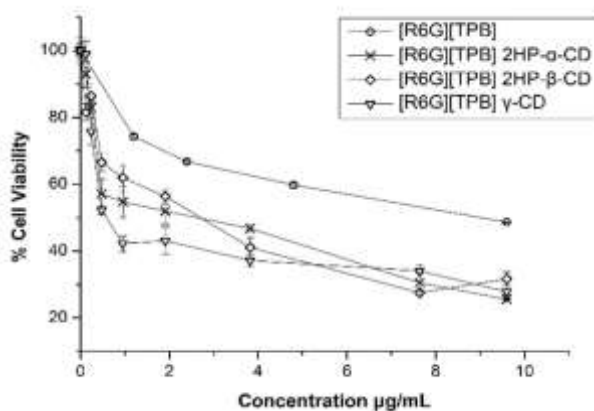


Figure 3. Toxicity of [R6G][TPB] nanoGUMBOS with and without cyclodextrin templating towards MDA-MB-231 breast cancer cells

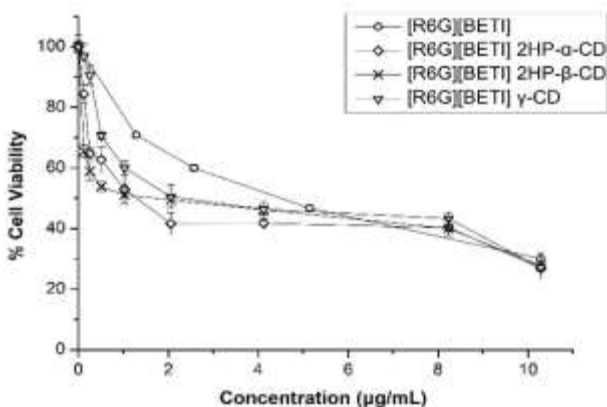


Figure 4. Toxicity of [R6G][BETI] nanoGUMBOS with and without cyclodextrin templating towards MDA-MB-231 breast cancer cells

Table 2. IC₅₀ concentrations [R6G][TPB] and [R6G][BETI] nanoGUMBOS towards MDA-MB-231 breast cancer cells and Mia Paca pancreatic cancer cells

Compound	IC ₅₀ µg/mL MDA-MB-231	IC ₅₀ µg/mL MiaPaca
[R6G][TPB] Control	7.3 ± 1.1	0.75 ± 0.05
[R6G][TPB] 2HP-α-CD	2.6 ± 0.2	0.37 ± 0.03
[R6G][TPB] 2HP-β-CD	2.7 ± 0.3	0.39 ± 0.06
[R6G][TPB] γ-CD	1.4 ± 0.3	0.24 ± 0.04
[R6G][BETI] Control	4.2 ± 0.4	0.45 ± 0.05
[R6G][BETI] 2HP-α-CD	1.6 ± 0.3	0.24 ± 0.03
[R6G][BETI] 2HP-β-CD	1.7 ± 0.2	0.26 ± 0.04
[R6G][BETI] γ-CD	2.3 ± 0.4	0.30 ± 0.03

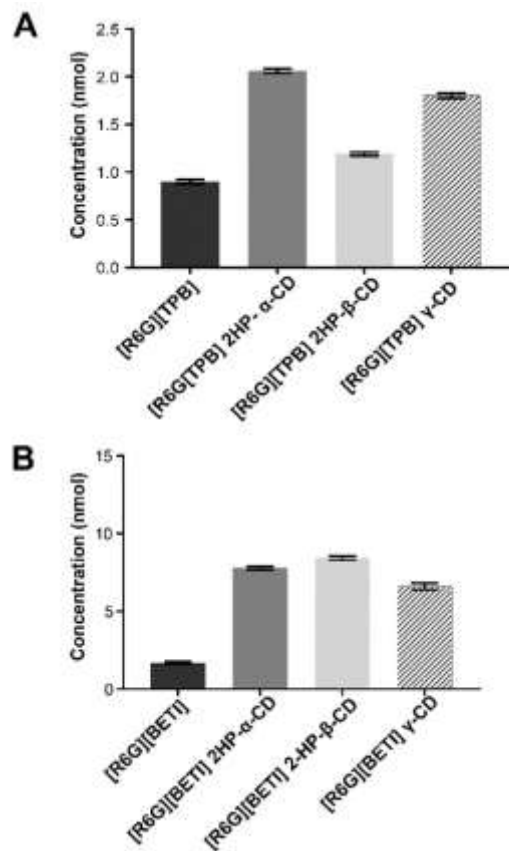


Figure 5. Cellular uptake of 5 μ M (A) [R6G][TPB] and (B) [R6G][BETI] nanoGUMBOS with and without cyclodextrin templating in MDA-MB-231 cancer cells after 5 h.

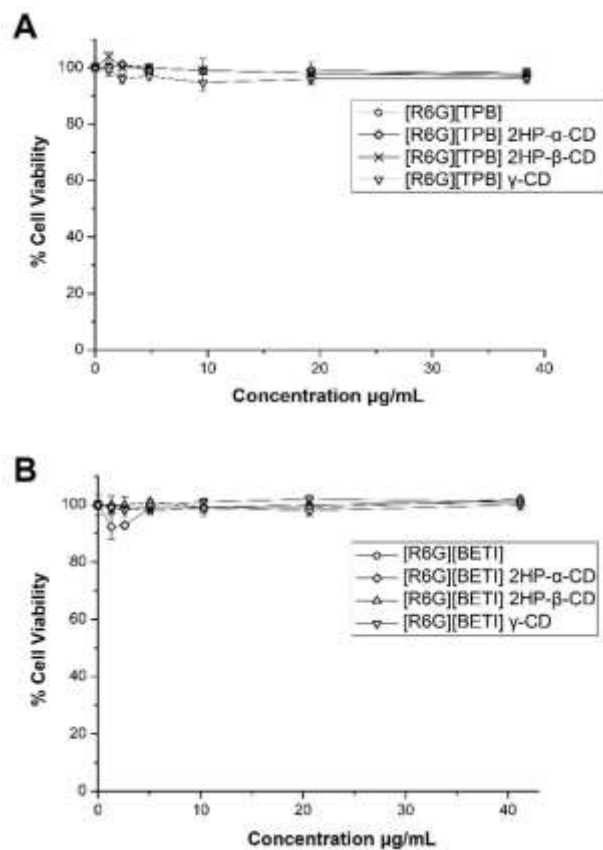
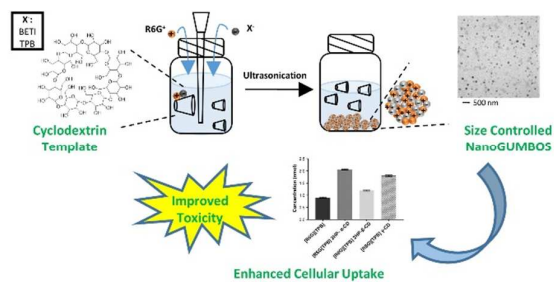


Figure 6. Toxicity of (A) [R6G][TPB] and (B) [R6G][BET] nanoGUMBOS with and without cyclodextrin templating towards Hs578Bst normal cells

Graphical Abstract:

Rhodamine 6G nanoGUMBOS were templated with cyclodextrin to develop size tunable nanodrugs with enhanced cellular uptake and selective chemotherapeutic toxicity.